Coordination Chemistry Reviews 254 (2010) 2459–2471

Contents lists available at ScienceDirect

Coordination Chemistry Reviews

journal homepage: www.elsevier.com/locate/ccr

Review

Integrating proton coupled electron transfer (PCET) and excited states

Christopher J. Gagliardi[a], Brittany C. Westlake[a], Caleb A. Kent[a], Jared J. Paul[b], John M. Papanikolas[a], Thomas J. Meyer[a,*]

[a] Department of Chemistry, University of North Carolina at Chapel Hill, Chapel Hill, NC 27599, United States
[b] Department of Chemistry, Villanova University, 800 Lancaster Avenue, Villanova, PA 19085, United States

Contents

ARTICLE INFO

Article history:
Received 26 November 2009
Accepted 4 March 2010
Available online 12 March 2010

Keywords:
Excited states
Proton coupled electron transfer
Electron–proton transfer
Solar fuels
Photosystem II
Artificial photosynthesis

ABSTRACT

In many of the chemical steps in photosynthesis and artificial photosynthesis, proton coupled electron transfer (PCET) plays an essential role. An important issue is how excited state reactivity can be integrated with PCET to carry out solar fuel reactions such as water splitting into hydrogen and oxygen or water reduction of CO_2 to methanol or hydrocarbons. The principles behind PCET and concerted electron–proton transfer (EPT) pathways are reasonably well understood. In Photosystem II antenna light absorption is followed by sensitization of chlorophyll P_{680} and electron transfer quenching to give P_{680}^+. The oxidized chlorophyll activates the oxygen evolving complex (OEC), a $CaMn_4$ cluster, through an intervening tyrosine–histidine pair, Y_Z. EPT plays a major role in a series of four activation steps that ultimately result in loss of $4e^-/4H^+$ from the OEC with oxygen evolution. The key elements in photosynthesis and artificial photosynthesis – light absorption, excited state energy and electron transfer, electron transfer activation of multiple-electron, multiple-proton catalysis – can also be assembled in dye sensitized photoelectrochemical synthesis cells (DS-PEC). In this approach, molecular or nanoscale assemblies are incorporated at separate electrodes for coupled, light driven oxidation and reduction. Separate excited state electron transfer followed by proton transfer can be combined in single semi-concerted steps (photo-EPT) by photolysis of organic charge transfer excited states with H-bonded bases or in metal-to-ligand charge transfer (MLCT) excited states in pre-associated assemblies with H-bonded electron transfer donors or acceptors. In these assemblies, photochemically induced electron and proton transfer occur in a single, semi-concerted event to give high-energy, redox active intermediates.

Published by Elsevier B.V.

1. Introduction

Essentially all chemical reactions of interest for energy conversion in chemistry and biology involve proton coupled electron transfer (PCET). In PCET both electrons and protons are transferred in the net reaction or half reaction. Energy conversion examples include the light driven water reduction of CO_2 to carbohydrates in natural photosynthesis, Eq. (1), water splitting in Eq. (2), and water reduction of CO_2 to methane (or other hydrocarbons) in Eq. (3):

$$6CO_2 + 6H_2O + 24h\nu \rightarrow C_6H_{12}O_6 + 6O_2 \quad (\Delta G^\circ = 29.1\,\text{eV}, n = 24) \tag{1}$$

$$2H_2O + 4h\nu \rightarrow 2H_2 + O_2 \quad (\Delta G^\circ = 4.92\,\text{eV}, n = 4) \tag{2}$$

* Corresponding author.
E-mail address: tjmeyer@unc.edu (T.J. Meyer).

0010-8545/$ – see front matter. Published by Elsevier B.V.
doi:10.1016/j.ccr.2010.03.001

$$[Ru^{IV}(bpy)_2(py)(O)]^{2+} \xrightarrow[\text{(vs. NHE)}]{0.78} [Ru^{III}(bpy)_2(py)(OH)]^{2+} \xrightarrow{0.67} [Ru^{II}(bpy)_2(py)(H_2O)]^{2+}$$

$$\Delta E^{o} = 0.11\ V$$

Scheme 1.

$$2H_2O + CO_2 + 8h\nu \rightarrow CH_4 + 2O_2 \quad (\Delta G^{\circ} = 10.3\,eV, n = 8) \qquad (3)$$

These reactions are at the heart of natural photosynthesis and of many schemes that utilize artificial photosynthesis for energy conversion [1–16]. They are complex due to their multi-electron character and occur by multi-step mechanisms, but common elements are required for successful implementation in actual working devices: *light absorption, excited state energy and electron transfer, electron/proton transfer driven by free energy gradients, electron transfer activation of catalysts for oxidation and reduction, product separation, and integration in spatially defined architectures*. There is a well-defined strategy for creating integrated structures in artificial photosynthesis. It is based on a "modular" approach in which individual components are designed, refined, and then assembled in integrated devices [4,5].

There is a clear delineation in this between a photovoltaic device, where the goal is to use solar energy to create a photopotential and drive a current through a load, and a photochemical or photoelectrochemical solar fuel device. The output from a photovoltaic device can be coupled to catalysts for oxidation and reduction with solar fuels produced by photoelectrolysis. This is an alternate approach but suffers in overall device efficiency which is the product of efficiencies for the sequential energy conversion and catalysis steps.

Direct chemical conversion in a solar fuels device could, in principle, achieve higher efficiencies but is a more complicated endeavor given the requirements posed by integrating multiple functions into a flexible architecture. Chemistry is at the heart of the matter with a major challenge in identifying robust catalysts for the multi-electron, multi-proton reactions in Eqs. (2) and (3). Rate is also a major consideration with the requirement for turnover rates near 1 ms at individual sites in order to make the rate of solar insolation, in photons per unit time, rate limiting.

In the chemical steps in photosynthesis and artificial photosynthesis, PCET and proton transfer play essential roles. Those roles need to be recognized, delineated, and designed into any successful device. Our understanding of the underlying principles and phenomena is evolving and enough is known to begin to document the role of PCET in solar fuel reactions. The coupling of PCET and solar fuel reactions provides the basis for this account.

The principles behind PCET and how it applies to catalysis will first be developed followed by a summary of how light absorption and proton management appear to be coupled in Photosystem II. The role of PCET in artificial photosynthesis will be illustrated and, finally, recent developments in direct photochemical electron–proton transfer, *photo*-EPT, described. The latter has important implications for photocatalysis and for driving solar fuel reactions.

2. Proton coupled electron transfer (PCET): introduction

PCET, reactions in which both electrons and protons are transferred, is at the heart of solar fuel reactions in chemistry and biology both thermodynamically and kinetically. They are multi-electron, multi-proton in nature, typically with significant kinetic barriers for pathways involving high-energy $1e^-$ or H^+ intermediates. Examples are water oxidation to hydroxyl radical with $E^{\circ}(OH^{\bullet}/H_2O) = 2.4\,V$ and $1e^-$ oxidation of tyrosine (TyrOH) to the radical cation without proton loss, $E^{\circ}(TyrOH^{\bullet+}/TyrOH) = 1.34\,V$.

PCET plays an important role thermodynamically by avoiding charge build up enabling multiple redox equivalents to be concentrated at single chemical sites or clusters over a narrow potential range. This is illustrated by the increase in E° of only 0.11 V at pH 7 for the sequential Ru(III/II), Ru(IV/III) PCET couples in Scheme 1. Scheme 1 illustrates oxidation of $Ru^{II}(bpy)_2(py)(OH_2)^{2+}$ (bpy is 2,2′-bipyridine; py is pyridine) to $Ru^{III}(bpy)_2(py)(OH)^{2+}$, and subsequent oxidation of $Ru^{III}(bpy)_2(py)(OH)^{2+}$ to $Ru^{IV}(bpy)_2(py)(O)^{2+}$ which are both $1e^-/1H^+$ couples with no charge build up. Typical $\Delta E^{\circ\prime}$ values of 0.5–1.5 V are observed between adjacent metal complex couples where there is charge buildup, an example being $\Delta E^{\circ\prime} = 1.7\,V$ between the Ru(IV/III) and Ru(III/II) couples $Ru(bpy)_2Cl_2^{2+/+}$ and $Ru(bpy)_2Cl_2^{+/o}$ in MeCN [17–19].

For PCET couples, oxidation leads to enhanced acidity, an example being a decrease in pK_a from 10.6 to 0.85 for $Ru^{III}–OH_2^{3+}$ cpasompared to $Ru^{II}–OH_2^{2+}$. This leads to proton loss when $Ru^{II}–OH_2^{2+}$ is oxidized above pH 0.85. Similarly, oxidation of $Ru^{III}–OH^{2+}$ to $Ru^{IV}{=}O^{2+}$ occurs over the entire pH range because the oxo complex has a very low proton affinity. In $Ru^{IV}(bpy)_2(py)(O)^{2+}$, Ru^{IV} is stabilized by $2p_{\pi}(O)$ donation with multiple bond formation, $Ru^{IV}{=}O$ [17,20,21].

Loss or gain of both electrons and protons by PCET is critical in catalyst activation. This point is also illustrated by the half reactions in Scheme 1. Sequential $1e^-/1H^+$ loss leads to the reactive, high oxidation state Ru(IV) oxo complex $Ru^{IV}(bpy)_2(py)(O)^{2+}$, Eq. (4). It is notable that oxidative activation in this case also meets half of the electron/proton loss requirements for water oxidation, $2H_2O \rightarrow O_2 + 4H^+ + 4e^-$:

$$Ru^{II}–OH_2^{2+} \xrightarrow{-2e^-,\,-2H^+} Ru^{IV}{=}O^{2+} \qquad (4)$$

There is also an important kinetic role for PCET in avoiding high-energy intermediates by use of concerted electron–proton transfer (EPT) pathways in which both electrons and protons are transferred simultaneously. An illustration of the energy barrier savings is seen in comparing oxidation of tyrosine (TyrOH) by $Os(bpy)_3^{3+}$ by the competing mechanisms in Eqs. (5) and (6) [22–24]. In Eq. (5) rate limiting electron transfer oxidation (ET) is highly unfavorable with $\Delta G^{\circ\prime} = +0.54\,eV$. ET is followed by proton transfer (PT) to the medium at the prevailing pH. In Eq. (6) electron transfer occurs to $Os(bpy)_3^{3+}$ (6a) in concert with proton transfer to HPO_4^{2-} with proton transfer occurring from TyrOH through a pre-formed H-bond (6b). Multiple site-electron proton transfer (MS-EPT) in Eq. (6b) occurs with $\Delta G^{\circ\prime} \sim 0\,eV$ at pH 7. MS-EPT is a concerted electron–proton transfer pathway with the electron and proton acceptors on chemically different sites:

$$Os^{III}(bpy)_3^{3+} + TyrOH \rightarrow Os^{II}(bpy)_3^{2+} + TyrOH^{\bullet+}$$
$$\Delta G^{\circ\prime} = +0.54\,eV \qquad (5a)$$

$$TyrOH^{\bullet+} \rightarrow TyrO^{\bullet} + H^+ \quad \Delta G^{\circ\prime} = -0.54\,eV(pH7) \qquad (5b)$$

$$2TyrO^{\bullet} \rightarrow (TyrO)_2$$

$$TyrOH + OPO_2OH^{2-} \rightleftharpoons TyrOH\cdots OPO_2OH^{2-} \qquad (6a)$$

$$Os^{III}(bpy)_3^{3+} + TyrOH\cdots OPO_2OH^{2-} \underset{\Delta G^{\circ\prime}\sim 0\,eV}{\longrightarrow} Os^{II}(bpy)_3^{2+} + TyrO\cdot + HOPO_2(OH)^- \qquad (6b)$$

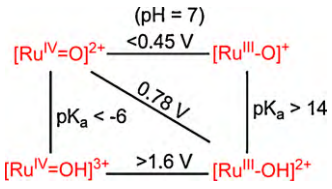

Scheme 2.

These effects play a significant role in catalyst activation. The example of oxidative activation of $Ru^{III}(bpy)_2(py)(OH)^{2+}$ to $Ru^{IV}(bpy)_2(py)(O)^{2+}$ is illustrated in the pK_a–E° diagram in Scheme 2. It shows that oxidation of Ru^{III}–OH^{2+} to catalytically active Ru^{IV}=O^{2+} occurs at 0.78 V at pH 7. However, for a pathway involving initial electron transfer, $E^\circ > 1.6$ V because of the high-energy, protonated oxo intermediate, Ru^{IV}=OH^{3+}. This imposes a significant barrier to $1e^-$ transfer which is manifested in large overvoltages for oxidizing $Ru^{III}(bpy)_2(py)(OH)^{2+}$ electrochemically, sluggish kinetics at electrodes, and relatively slow rates of electron transfer.

Developing reaction pathways that avoid the high-energy barriers imposed by initial ET or PT is essential to the success of solar fuel devices. This is a key feature the design of integrated devices which combine light absorption with catalysis.

That this is not an afterthought is illustrated by the complex sequence of EPT and proton transfer events and pathways that have been suggested to occur in Photosystem II (PSII) as described in the next section. In PSII, the molecular level catalyst for water oxidation is imbedded in the low dielectric thylakoid membrane without direct access to aqueous interfaces at the outer (stroma) and inner (lumen) sides of the membrane, Fig. 1. Proton management is key. It plays an important role in local EPT reactivity and in long-range proton transfer for proton equilibration and to remove protons released upon water oxidation. Both are essential to the successful operation of the oxygen evolving complex (OEC) appearing to play a major role, even dominating the structure. The reaction center of Photosystem II has been described as 'an intricate structure that is "wired for protons"' [25].

3. Proton coupled electron transfer (PCET) and concerted electron–proton transfer in Photosystem II

Photosynthesis in green plants occurs in ~5 μm ellipsoidal cellular structures, called chloroplasts, with 1–1000 chloroplasts found in the cell walls of green plants. The photosynthetic apparatus is found inside the chloroplast, largely imbedded in the walls of the thylakoid compartment. As shown in Fig. 1, from Wikipedia, the membrane houses four of five key functional elements required for photosynthesis to occur [26]. Four are imbedded in the membrane: *Photosystem II*, where light driven water oxidation occurs; intervening protein b_6f, which transfers electrons through free energy gradients releasing protons to the inside of the compartment, the lumen; *Photosystem I* where light driven reduction of $NADP^+$ to NADPH occurs; and *ATP Synthase* where the proton gradient built up in the lumen is used to convert ADP to ATP for energy storage. CO_2 reduction in the *Calvin Cycle* occurs in a structure external to the stroma driven by NADPH produced in Photosystem I.

As shown in Eq. (7), the sum of the two light reactions in photosynthesis produces O_2 and NADPH, storing an impressive 4.56 eV of chemical energy. The photosynthetic process also produces 7 ATPs with 7.5 kcal/mol stored/ATP.

$$2NADP^+ + 2H_2O + 4h\nu \rightarrow 2NADPH + O_2 + 2H^+ \quad ,$$
$$\Delta G^\circ = 4.56\,eV + \sim 7(ADP + P_i \rightarrow ATP) \qquad (7)$$

Photosynthesis is a spectacular example of PCET in action. In addition to the demands of the individual half reactions, e.g., $NADP^+ + 2e^- + H^+ \rightarrow NADPH$, with $E^\circ = -0.32$ V, ~12 protons are transferred across the membrane from the stroma to the lumen per O_2 produced. The resulting pH gradient is used to drive ATP production. Proton management in and through this largely hydrophobic environment is clearly a major issue in this "intricate structure wired for protons" [25].

As discussed in the abbreviated account below, the proton wiring in PSII appears to provide the mechanistic requirements for both EPT and long-range proton transfer. The latter is required for local proton equilibration. Protons are released by the OEC to the inner compartment or lumen over a distance of ~30 Å. Proton transfer occurs in ~10 μs through a long-range proton transfer channel by a series of local proton exchanges between neighboring carboxylates lining the proton transfer channel.

Oxygen evolution occurs following four sequential light absorption–electron transfer activation steps as summarized in the modified "Kok" cycle in Scheme 3. In this cycle, activation of the OEC results in a series of PCET oxidation steps each driven by single photon absorption. The OEC progresses from initial state S_0 to final state S_4 where oxygen evolves. S_4 is reached following loss of $4e^-$ and $4H^+$ with the protons transferred to the lumen. After O_2 loss, the catalytic system is reset for another light-driven cycle.

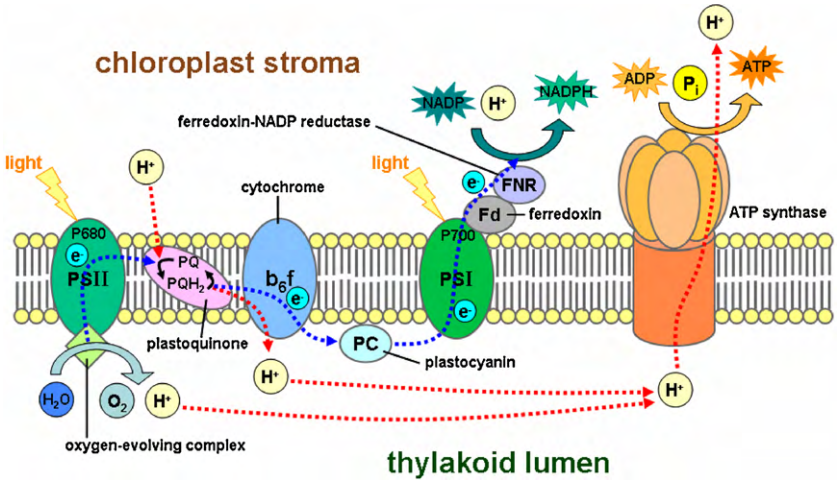

Fig. 1. Schematic illustration of the thylakoid membrane of photosynthesis showing the integrated components of the photosynthetic apparatus [29].

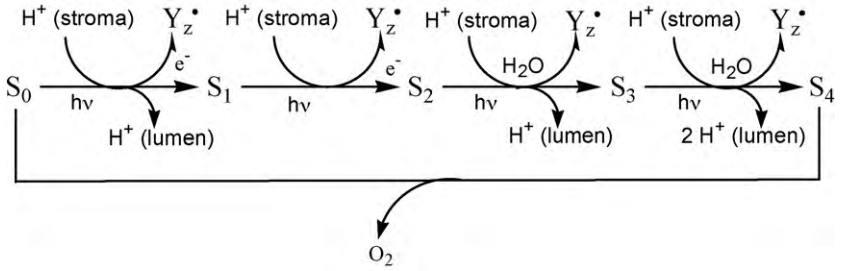

Scheme 3. Modified Kok cycle for water oxidation in PSII.

Water oxidation in the OEC also drives the entry of $4H^+$ into the membrane from the stroma. They are used in PCET reduction of a quinone/hydroquinone couple (plastoquinone to plastoquinol). Following reduction, plastoquinol transports reductive equivalents to b_6f, Fig. 1.

The XRD structure of PSII has been determined to 3 Å resolution [27,28]. At the heart of the structure is the reaction center shown in Fig. 2 where light harvested in a complex, membrane-bound antenna structure is funneled to chlorophyll P_{680} giving its lowest singlet excited state, P_{680}^*. P_{680}^* undergoes oxidative quenching to give P_{680}^+. It subsequently initiates a sequence of events culminating in an oxidative equivalent appearing in a $CaMn_4$ cluster in the oxygen evolving complex (OEC). Following absorption of four photons and accumulation of four oxidative equivalents, oxygen is evolved.

The initial sequence of events following single photon sensitized formation of P_{680}^* is shown in Fig. 2. Following formation of P_{680}^*, rapid (~1 ps) oxidative quenching occurs by electron transfer quenching by neighboring pheophytin $Pheo_{D1}$. Quenching is followed by electron transfer to neighboring quinone, Q_A. This sequence of reactions results in conversion of a 1.8 eV excited state into ~1.4 eV of transiently stored free energy in the redox separated state, $Q_A^{\bullet-}$–P_{680}^+. In this state the reductive and oxidative equivalents are separated by 17–18 Å. Importantly, the oxidative equivalent at P_{680}^+ is a powerful oxidant with $E^{\circ'}(P_{680}^+/P_{680}) = 1.2$ V well capable of water oxidation with $E^{\circ'}(O_2/H_2O) = 0.82$ V at pH 7.

The oxidative equivalent produced in the quenching step is ultimately transferred to the OEC where water oxidation occurs. Oxidative activation of the OEC occurs stepwise by oxidation of an intermediate tyrosine–histidine pair, Y_Z, Fig. 2. As shown in Fig. 2, oxidation of Y_Z, $Q_A^{\bullet-}$–P_{680}^+–$Y_Z \rightarrow Q_A^{\bullet-}$–$P_{680}$–$Y_Z^{\bullet+}$, is relatively slow with $k \sim 10^7\ s^{-1}$. Nonetheless, it occurs with a high per photon absorbed efficiency with $\eta \sim 0.9$. The high efficiency is a consequence of slow back electron transfer, $Q_A^{\bullet-}$–$P_{680}^+ \rightarrow Q_A$–$P_{680}$, with $k \sim 7 \times 10^3\ s^{-1}$. Back electron transfer is slow due the relatively long distance involved, 17–18 Å, and because the reaction is highly favored, $\Delta G^{\circ'} \sim -1.4$ eV, and occurs in the *inverted region*. In this region, electron transfer rates decrease as the driving force increases. *Without the inverted region and its role in slowing back electron transfer in this reaction, life as we know it would not exist on the planet*.

The intermediate oxidation of Y_Z by P_{680}^+, before oxidative activation of the OEC occurs, is critical to the efficient operation of the reaction center. It further increases the separation distance between oxidative and reductive equivalents from 17 to 18 Å in $Q_A^{\bullet-}$–P_{680}^+ to ~35 Å in $Q_A^{\bullet-}$–$Y_Z^{\bullet+}$. The increase in distance is important because it further slows back electron transfer, in this case from $Q_A^{\bullet-}$ to $Y_Z^{\bullet+}$, $Q_A^{\bullet-}$–$Y_Z^{\bullet+} \rightarrow Q_A$–$Y_Z$. Back electron transfer is a deleterious step resulting in wasted redox equivalents and local heating rather than contributing to water oxidation.

Back electron transfer from $Q_A^{\bullet-}$ to $Y_Z^{\bullet+}$ is in competition with $Y_Z^{\bullet+}$ oxidative activation of the OEC, OEC–$Y_Z^{\bullet+} \rightarrow$ OEC$^{\bullet+}$–Y_Z. This the step which initiates the water oxidation cycle. The time scale for OEC activation is relatively slow, 0.1–1 ms, depending on the step in the Kok cycle, $S_0 \rightarrow S_1$, $S_1 \rightarrow S_2$, ... This makes it imperative to minimize back electron transfer by slowing it even further. Taking no chances, still another electron transfer occurs, in this case between $Q_A^{\bullet-}$ and neighboring quinone – Q_B (plastoquinone PQ, whose structure is shown below) – in 0.2–0.4 ms. This last step increases the back electron transfer distance to >50 Å opening an even longer time window for OEC activation. Electron transfer between $Q_A^{\bullet-}$ and Q_B is coupled to proton transfer from the stroma to a neighboring glutamate (Glu^-).

The overall sequence of light-driven reactions occurring in the first, $S_0 \rightarrow S_1$, stage of photosynthesis is illustrated in Eq. (8). Fur-

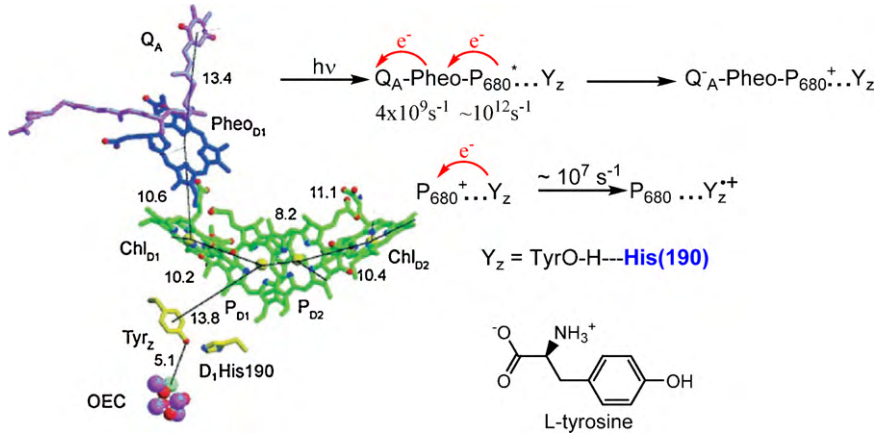

Fig. 2. Structure of the reaction center in Photosystem II and the initial light-driven reactions. Reproduced in part with permission from Ref. [30]. Copyright 2004 American Association for the Advancement of Science.

ther reduction of $Q_B^{\bullet -}$ occurs in the second stage, $S_1 \rightarrow S_2$. Addition of a second electron to $Q_B^{\bullet -}$ is accompanied by H^+ transfer from GluH. In addition, a second proton is transferred from the stroma to give the reduced quinol, H_2Q_B (PQH_2). Once formed, H_2Q_B diffuses through the membrane to the b_6f complex where it is reoxidized to Q_B. The released protons are transferred to the lumen. The initial reductive equivalent is ultimately transferred to PSI as the reduced Cu(I) form of plastocyanin.

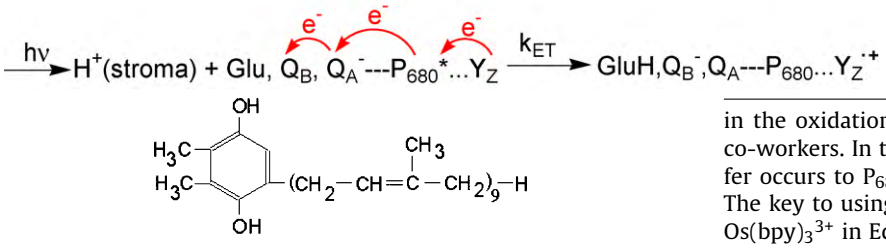

H_2Q_B (PQH_2).

The sequence of electron transfers in Eq. (8) leaves the oxidative equivalent at Y_Z as $Y_Z^{\bullet +}$ with sufficient time to activate the OEC which, as noted above, occurs on the 0.1–1 ms timescale depending on the stage in the Kok cycle. As shown in the structure in Fig. 2, Y_Z is a combination of a phenol, tyrosine Tyr_Z, and an adjacent base, Histidine 190. Although seemingly innocuous, the presence of His190 is essential for water oxidation. Site directed mutagenesis studies show that once His190 is removed *water oxidation no longer occurs* [31–33]!

The importance of His190 provides clear, if inferential, evidence for the importance of Multisite electron–proton transfer (MS-EPT)

(8)

in the oxidation of Y_Z to Y_Z^+ as first suggested by Babcock and co-workers. In this pathway, illustrated in Eq. (9), electron transfer occurs to P_{680}^+ with simultaneous proton transfer to His190. The key to using MS-EPT in this case, as in tyrosine oxidation by $Os(bpy)_3^{3+}$ in Eq. (6b), is the relative driving force of EPT relative to other pathways. EPT in Eq. (9) is favored by ~0.4 eV over ET in Eq. (10) due to the high-energy of the tyrosine radical cation, $E^{\circ\prime}(TyrOH^{\bullet +/0}) = 1.34$ V. His190 introduces a low energy EPT pathway enhancing Y_Z oxidation and allowing photosynthesis to occur. *EPT plays a pivotal role in PSII similar to the role played by the inverted region.*

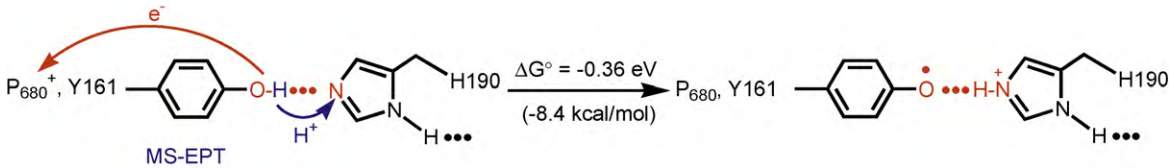

(9)

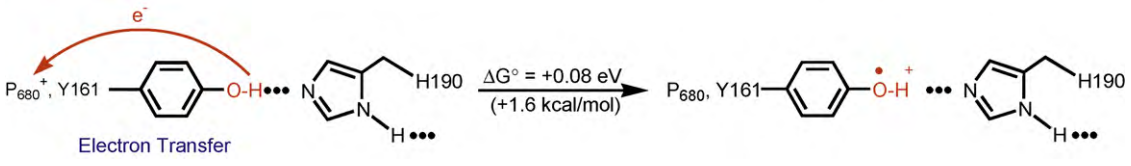

(10)

EPT and proton transfer also appear to play critical roles in subsequent steps in the Kok cycle both by avoiding high-energy ET and PT intermediates and by removing protons released by water oxidation. The structure of the OEC, as determined by EXAFS and

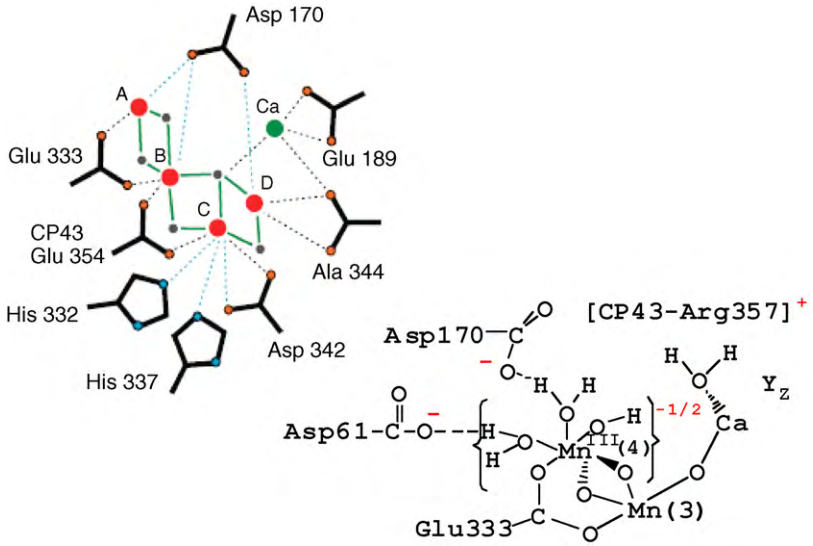

Fig. 3. 3 Å XRD/EXAFS structure of the OEC, upper left, and the proposed structure of the catalytically active Mn site, Mn(4). Reproduced with permission from Ref. [25,28]. Copyrights 2007 Wiley-VCH Verlag GmbH & Co. and 2006 American Association for the Advancement of Science.

XRD to 3 Å resolution, is shown in Fig. 3, as is a fragment of the OEC thought to be the reactive region for water oxidation and oxygen evolution. A key element is the presence of Y_Z at a distance of ~7 Å from the nearest Mn site in the cluster, Mn(4) [20]. Mn(4) appears to be the key Mn site for oxygen evolution. In the structure of the OEC in Fig. 3, it is tied to the remaining $CaMn_3$ cluster by two bridging μ-oxo groups and a bridging glutamate.

Additional key structural elements for water oxidation appear in the OEC fragment in Fig. 3 [27,28]. Aspartate 61 (Asp61) is the known entryway to a proton exit channel that transfers protons released in the reaction center to the lumen on the inner side of the membrane. In Fig. 3 it is shown H-bonded to a coordinated H_2O molecule which is not distinguishable in the 3 Å structure. Another water molecule (not distinguishable) is shown bound to the Ca of the OEC cluster aligned toward a Mn–OH_2 axis at Mn(4). This is the spatial region in the structure where O–O bond formation is thought to occur, see below. A last structural feature of note is Mn(3) which acts as the connector to the remaining $CaMn_3$ cluster. It, or a delocalized cluster orbital, have been suggested to play a role in the oxidative chemistry in addition to serving as a structural element, see below:

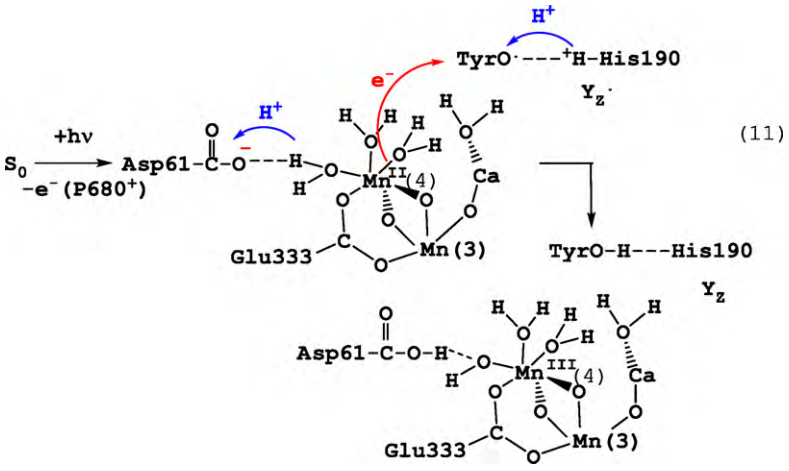

(11)

EPT has been suggested to play an equally important role in oxidative activation of the OEC. The first, $S_0 \rightarrow S_1$, stage of the Kok cycle has been suggested to occur by EPT by a special pathway involving simultaneous $1e^-/2H^+$ transfer, Eq. (11). In this pathway, $1e^-$ transfer occurs to the tyrosyl radical in $Y_Z^{\bullet+}$ from $Mn^{II}(4)$ in concert with back H^+ transfer from His190: Mn^{II}–$Tyr_ZO^{\bullet}\cdots{}^+$H-His190 → Mn^{III}–Tyr_ZO–H···His190. The back-and-forth movement of the proton between Tyr_Z and His190 has been referred to as "proton rocking" by Renger.

In the $1e^-/2H^+$ pathway, electron transfer occurs from $Mn^{II}(4)$ to $Y_Z^{\bullet+}$. It has been suggested that this part of the reaction also utilizes MS-EPT with $1e^-$ transfer to $Y_Z^{\bullet+}$ occurring in concert with $1H^+$ transfer to Asp61: Asp(61)$COO^-\cdots$H–O(H)–Mn^{II}, $Y_Z^{\bullet+} \rightarrow$ Asp(61)COO–H···O(H)–Mn^{III}, Y_Z. EPT in this case avoids a high-energy Mn^{III}–OH_2 intermediate. A significant decrease in pK_a is predicted upon oxidation of Mn^{II}–OH_2 to Mn^{III}–OH_2. For the corresponding aqua complexes, $Mn(OH_2)_6^{3+/2+}$, $\Delta pK_a = 10.7$ [25,34,35]. ET oxidation of $Mn^{II}(4)$ without concerted proton transfer has been estimated to be a more energetic pathway by ~8 kcal/mol.

In the concerted pathway in Eq. (11) a proton is transferred from the $CaMn_4$ cluster to Asp61 which, as noted above, is the entryway to a proton exit channel. The released proton is subsequently transferred through this channel ~30 Å to the lumen in ~1 μs, reaction (1) in Eq. (12) [20].

Even with loss of the proton, there is still a proton structural imbalance in once-oxidized S_0 due to the loss of the H-bond between Mn(4)–OH_2 and Asp61. Further, the –OH ligand at Mn(4) is oriented away from the Ca of the cluster core where O···O bond formation is thought to occur. Consequently, it has been suggested that the final step in the $S_0 \rightarrow S_1$ transition at the OEC involves a –OH/–OH_2 cross-coordination sphere proton transfer, reaction (2) in Eq. (12), driven, in part, by reforming the H-bond with Asp61. With this final step, S_1 is fully formed, ready to advance further in the Kok cycle.

(11)

(12)

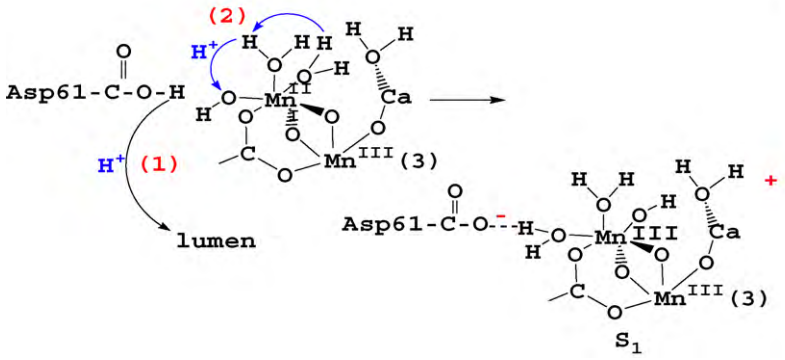

(12)

The series of reactions that occur in the OEC during the $S_0 \rightarrow S_1$ transition are summarized in Eq. (13). It highlights the fact that single photon absorption induces and drives a remarkably extensive sequence of coupled reactions. In the net sense single photon absorption results in $1e^-$ loss from the OEC, internal displacement

of a H^+ from $Mn–OH_2$ to Glu, and net H^+ is transfer across the membrane from the stroma to the lumen contributing to the pH gradient for ATP production.

$$(Q_B, Q_A), Glu^- – P_{680} \cdots Y_Z \cdots S_0(Mn^{II}–OH_2) + H^+(stroma) + h\upsilon \rightarrow (Q_B^-, Q_A), GluH–P_{680} \cdots Y_Z \cdots S_1(Mn^{III}–OH) + H^+(lumen) \quad (13)$$

Similarly impressive, coupled PCET/EPT sequences have been proposed for the remaining steps in the Kok cycle as documented in Refs. [20,25] and elsewhere. Single photon driven reactions at $S_1 \rightarrow S_2$ and $S_2 \rightarrow S_3$ have been proposed to lead to high oxidation state, $Mn^{IV}(3)Mn^{IV}(4)$=O, at the OEC. Oxidation of $Mn^{III}(3)$, or a delocalized cluster orbital, appears to occur in the $S_1 \rightarrow S_2$ stage. This is followed by additional electron loss in $S_2 \rightarrow S_3$ to give $Mn^{IV}(3)Mn^{IV}(4)$=O.

It has been proposed that $Mn^{IV}(3)Mn^{IV}(4)$ O is the key intermediate in which O···O bond formation occurs, Eq. (14). In this pathway the second O-atom for O···O coupling is thought to come from the coordination sphere of the Ca of the $CaMn_4$ cluster, Eq. (14). As shown in Eq. (14) this may involve Ca–OH with coordinated OH^- formed in a preceding acid–base equilibrium with neighboring Asp170. There may also be a concerted atom–proton transfer step with Asp170 acting as the acceptor base.

$$Mn^{IV}(3)Mn^{IV}(4)=O, HO–Ca + H_2O \rightarrow Mn^{III}(3)Mn^{III}(4)OOH, H_2O–Ca \quad (14)$$

The Kok cycle is completed by further $1e^-/1H^+$ oxidation of the intermediate Mn^{III}–OOH and release of O_2 which occurs in the terminal stage of the Kok cycle following the $S_3 \rightarrow S_4$ transition.

4. Proton coupled electron transfer (PCET) and electron–proton transfer (EPT) in artificial photosynthesis and solar fuels

Although most schemes for a sustainable energy future rely heavily on solar energy, without a means for energy storage on massive scales, solar energy can never be successful as a primary energy source. The sun is a locally intermittent energy source. Energy storage is required at night when the sun is no longer available.

The implied requirements for short-term energy storage are vast. Current energy consumption globally is >13 TW (terrawatt) with 1 TW = 10^9 kW. The only feasible solution to energy storage at that level appears to be solar fuels and the energy stored in chemical bonds. Candidate reactions are water splitting in Eq. (2) and solar driven water reduction to methanol, methane, or other hydrocarbons, Eq. (3). The latter are especially attractive since they could be utilized within the existing energy infrastructure.

Artificial photosynthesis addresses this problem by attempting to incorporate the essential elements of photosynthesis, with its underlying molecular/nanoscale events, in integrated nanoscale and molecular level architectures. A systematic "modular" approach is available in which individual elements for each function are studied separately and then integrated in molecular assemblies or nanoscale arrays. A generic *excited state or dye sensitized photoelectrochemical cell* (DS-PEC) is shown in Fig. 4. As in a dye sensitized photovoltaic solar cell (DSSC), it features molecular excitation and excited state formation at chromophores chemically attached to semiconductor surfaces. However, in a DS-PEC, photoproduced redox equivalents are used to drive chemical reactions rather than create a photopotential and photocurrent [36–38].

In the example in Fig. 4, excited state formation is followed by rapid electron transfer injection from the excited state into the conduction band of the semiconductor. This provides reductive equivalents to a cathode for catalyzed reduction of H^+ to H_2 or of

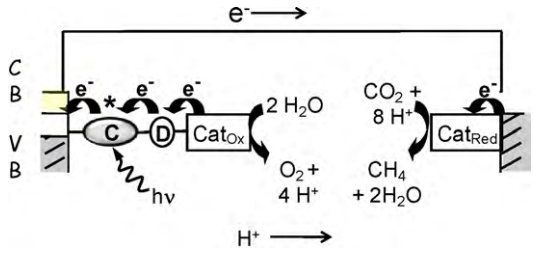

Fig. 4. Dye sensitized photoelectrochemical synthesis cell (DS-PEC) for CO_2 reduction [4]. C is a chromophore, D an intervening electron transfer donor, and Cat_{ox} and Cat_{red} are catalysts for water oxidation and reduction.

CO_2 to methanol or hydrocarbons. Reduction to methane is shown in Fig. 4. The band gap and absence of redox levels between conduction and valence bands is an essential feature provided by the semiconductor. The absence of intervening energy levels creates a built in inhibition to back electron transfer. Inhibition is required for any successful device where multiple redox equivalents must be concentrated at single sites or clusters that carry out multi-electron solar fuel reactions. An additional advantage is that the redox products, O_2 and CH_4 in Fig. 4, are physically separated avoiding direct or surface catalyzed back reactions.

The DS-PEC device in Fig. 4 is the solar driven reverse of a CH_4/O_2 fuel cell with solar energy used to drive the reaction in the non-spontaneous direction. The design is impressively straightforward compared to natural photosynthesis and is consistent with the design mantra *KEEP IT SIMPLE* required for a functional device.

A specific example of a surface-bound chromophore–quencher assembly for water oxidation is illustrated in Fig. 5. This molecule, $[(4,4'(HO)_2OPCH_2)_2bpy)_2Ru^{II}(bpm)Ru^{II}(Mebimpy)(OH_2)]^{4+}$(bpm is 2,2′-bipyrimidine; Mebimpy is 2,6-bis(1-methylbenzimidazol-2-yl)pyridine) combines the functions of light absorber and water oxidation catalyst in a single assembly. It can be attached to oxide surfaces (ITO (In_2O_3:Sn), FTO (SnO_2:F), or TiO_2) by hydrolytically stable phosphonate surface binding [39].

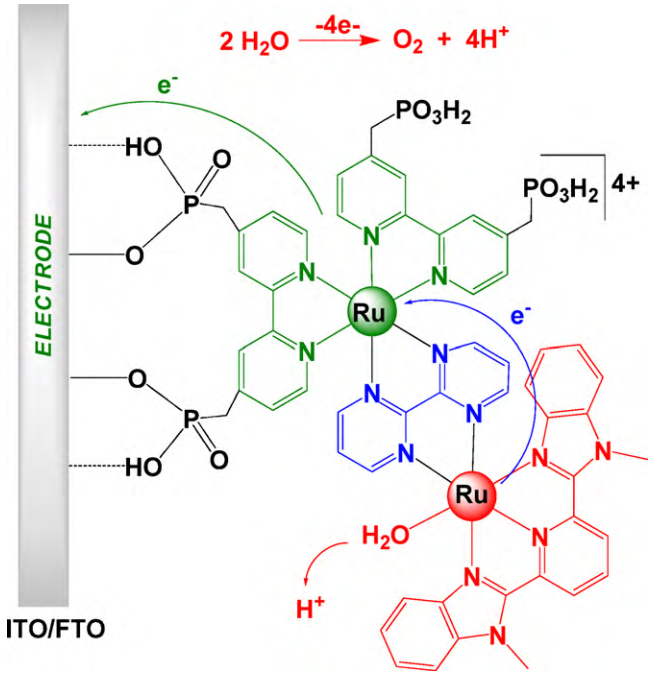

Fig. 5. Structure of surface-bound chromophore-quencher assembly, $[(4,4'(HO)_2OPCH_2)_2bpy)_2Ru^{II}(bpm)Ru^{II}(Mebimpy)(OH_2)]^{4+}$, illustrating PCET oxidative activation. Reproduced with permission from [40]. Copyright 2009 Wiley-VCH Verlag GmbH & Co.

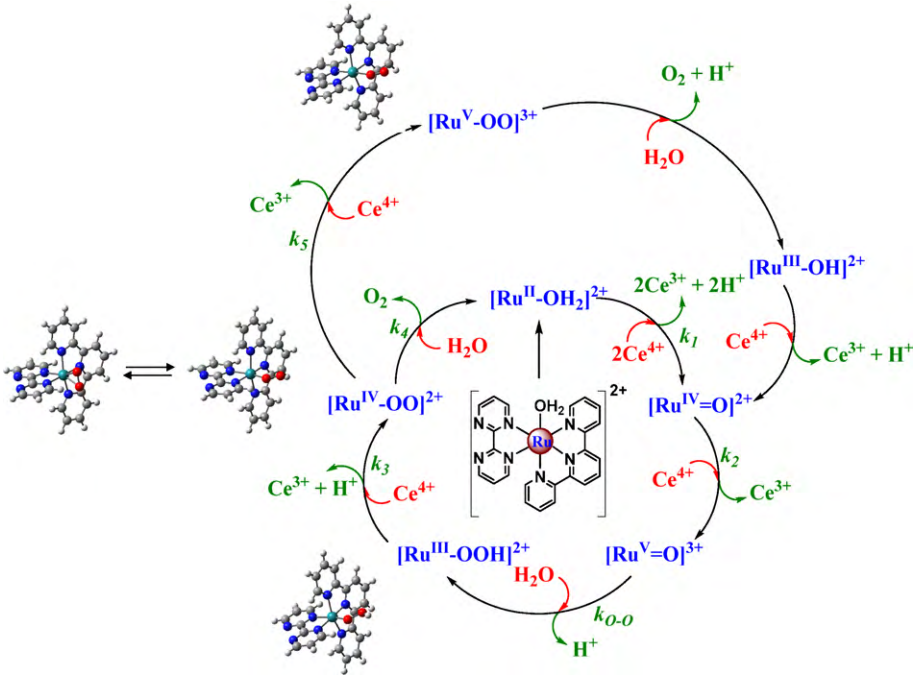

Scheme 4. Mechanism of Ce(IV) water oxidation catalyzed by Ru(tpy)(bpm)$(OH_2)^{2+}$ in 1.0 M HNO_3 at 25 ± 2 °C illustrating structures of proposed peroxidic intermediates [43].

Electrochemical measurements on conducting ITO or FTO electrodes reveal that the chromophore–quencher assembly retains the PCET redox properties of related monomeric water oxidation catalysts such as Ru(tpy)(bpz)$(H_2O)^{2+}$ (tpy is 2,2′:6′,2″-terpyridine; bpz is 2,2′-bipyrazine) and Ru(Mebimpy)(bpy)$(H_2O)^{2+}$. In these complexes, oxidative activation occurs by sequential PCET oxidation of Ru^{II}–OH_2^{2+} first to Ru^{III}–OH^{2+} and then to Ru^{IV}=O^{2+}. Further oxidation to Ru^V=O^{3+} is followed by O-atom transfer to solvent H_2O to give an intermediate peroxide, Ru^{III}–OOH^{2+}. The peroxide undergoes further oxidation to $Ru^{IV}(OO)^{2+}$ followed by oxygen release. The series of reactions that occur are summarized in Scheme 4. Structures of key intermediates calculated by DFT are also shown in the scheme.

As in PSII, the catalytic cycle in Scheme 4 advances by sequential loss of electrons and protons in a series of discrete chemical steps. The challenges are similar to those faced by PSII with extensive involvement of PCET, requirements for building up multiple redox equivalents, and long-range proton transfer coupled to electron transfer. The latter is far more straightforward in an interfacial, aqueous DS-PEC environment compared to the hydrophobic thyalkoid membrane. Separation of products can be achieved by use of a proton permeable membrane such as Nafion which is used in PEM fuel cells.

Initial reports of photochemically driven reactions in DS-PEC and related devices have appeared. An initial report appeared on dehydrogenation of *iso*-propanol to acetone, Eq. (15) [41]. A more recent report has appeared on water splitting with water oxidation based on IrO_2 nanoparticles as water oxidation catalysts [42]. Experiments on water splitting by using surface-attached chromophore-catalyst assemblies are ongoing.

$$(CH_3)_2CHOH + 2h\nu \rightarrow (CH_3)_2C{=}O + H_2 \quad (15)$$

5. Photochemical electron–proton transfer (*photo*-EPT)

In both photosynthesis and artificial photosynthesis, sequential light absorption/electron transfer/proton transfer steps are used to activate catalysts for solar fuel reactions. Net photochemical transformations are induced by light absorption followed by electron transfer and then by PCET to activate catalysts and drive thermal reactions. The "modular" approach provides a basis for developing components for separate functions, combining them later in integrated devices.

A considerable simplification in design could be achieved by combining electron and proton transfer in a single excitation event to give high-energy, redox active intermediates (*photo*-EPT). There are two significant issues to deal with. The first is to demonstrate that the phenomenon exists. Can *photo*-EPT occur and be demonstrated? The second, and perhaps more important is, can photochemical EPT be used for new photochemistry and, more to the point, can it be harnessed to drive solar fuel reactions?

5.1. Photochemical electron–proton transfer (photo-EPT) in hydrogen-bonded organic charge transfer excited states

At first glance, photochemical EPT would appear to be ruled out on fundamental grounds. According to the Franck–Condon principle, electronic excitation occurs rapidly on the timescale for nuclear motions, including proton movement. A concerted event, as described for thermal EPT, with electron and proton transfer occurring between equilibrium coordinate positions simultaneously is not possible.

In thermal EPT, with even nominal electronic coupling between donor and acceptor, simultaneous e^-/H^+ transfer is time-gated by the motion of the proton which is quantized. Both electron and proton transfer are quantum phenomena described by wave functions and wave function overlaps. The pre-exponential factor for the concerted process in a vibronic transition between initial vibrational level χ_v and final level $\chi_{v'}$, ν_{EPT}, in the limit of weak-to-moderate electronic coupling is given by Eq. (16) [44,45]. In Eq. (16), H_{ab} is the electron transfer matrix element. The second term is the square of the vibrational overlap integral for the transferring proton between its initial and final states. It gives the extent to which the initial and final states are coincident along the proton

transfer coordinate. For proton transfer within an unsymmetrical H-bond, A–H···B → A$^-$···$^+$H–B, the vibrational overlap integral is small falling off rapidly with the distance between initial and final equilibrium positions:

$$\nu_{EPT} = (2\pi H_{ab}^2/\hbar)\langle\chi_{v'}|\chi_v\rangle^2 \quad (16)$$

Electronic excitation at the molecular level results in instantaneous redistribution of electron density on the vibrational time scale. Once formed, the nuclei relax to the equilibrium nuclear configurations of the excited state both vibrationally and in the polarization distribution of the surrounding solvent. These are uncorrelated motions and occur on different time scales.

A related excitation–relaxation sequence provides the basis for a photochemical analog of thermal EPT, photo-EPT. The example of an excited donor–acceptor complex containing a dissociable proton H-bonded to acceptor base B, A–D–H···B, is illustrated in Eq (17). In this case intramolecular charge transfer (ICT) excitation leads to a new excited state electronic distribution, A$^-$–D–$^+$H···B, in which proton transfer is highly favored.

$$A–D–H\cdots B \xrightarrow{h\nu} \{A^- – D^+ – H\cdots B\}* \rightarrow (A^- – D\cdots H^+ – B)* \quad (17)$$

Excitation is a vertical process along the coupled nuclear coordinates including the transfer coordinate for the proton. In the initial ICT-EPT excited state, the proton is initially frozen in the equilibrium coordinate of the ν(O–H) coordinate of the ground state. It is highly elongated from the equilibrium coordinate of the ν(B–H) mode in the equilibrated ICT-EPT photoproduct. Proton transfer occurs as a redistribution along the proton transfer coordinate to the equilibrium coordinate for ν(B–H) in A$^-$–D···$^+$H–B. It is followed by relaxation in the other coupled vibrational and solvent modes to give the final thermally equilibrated ICT-EPT excited state with proton transfer complete.

Photo-EPT is analogous to rapid intramolecular proton transfer in certain types of excited states. It is related to proton transfer from thermally equilibrated excited states with the distinction a matter of timescale. In photo-EPT the proton transfers on a time scale that is short compared to relaxation of coupled intramolecular vibrational and solvent dipole modes. In excited state proton transfer, proton transfer occurs following vibrational and solvent relaxation. Photo-EPT is related to photochemical electron transfer. An example of the latter is intervalence transfer (IT) in mixed valence molecules, note the example of biferrocenium monocation in Eq. (18). In this case, absorption of a photon results in a new state in which an electron is transferred between sites followed by vibrational and medium relaxation. In *photo*-EPT, light absorption and internal charge redistribution lead to a new state in which light induced electron transfer is followed by motion of the proton where both occur before vibrational and medium relaxation.

$$(C_5H_5)Fe^{II}(C_5H_4–C_5H_4)Fe^{III}(C_5H_5)^+ \xrightarrow{h\nu} \{(C_5H_5)Fe^{III}(C_5H_4–C_5H_4)Fe^{II}(C_5H_5)^+\}^* \rightarrow (C_5H_5)Fe^{III}(C_5H_4–C_5H_4)Fe^{II}(C_5H_5)^+ \quad (18)$$

There are classes of molecules for which the change in electronic configuration between ground and excited state leads to significant changes in proton affinity and pK_a. One is substituted phenols where excited state "super acids" have been identified, note the examples below. The pK_a* for the excited state of the dicyanonaphthol is −5.2 [46]:

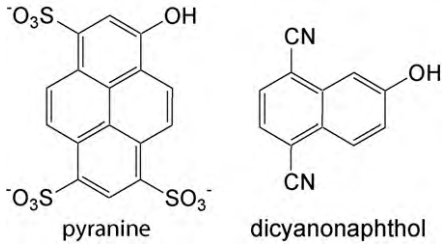

pyranine dicyanonaphthol

We have investigated *photo*-EPT in the *p*-nitrophenyl–phenol (O_2N–OH) shown in Eq. (19) [47]. An absorption band appears for this molecule at 337 nm in 1,2-dichloroethane (DCE) arising from an internal charge transfer (ICT) transition as assigned by DFT calculations. ICT excitation occurs from a $n\pi$ orbital with considerable –OH character to a π^* orbital largely –NO_2 in character. From the results of femtosecond transient absorption measurements, the initial $^1(n\pi^*$ICT) singlet state formed by absorption undergoes rapid S → T interconversion ($\tau \sim 3$ ps) followed by excited state decay of the triplet with $\tau = 2.4$ μs. Based on spectroscopic measurements and application of the Förster equation, it has been estimated that the acidity of the ICT excited state is increased by ~9 pK_A units in the excited state.

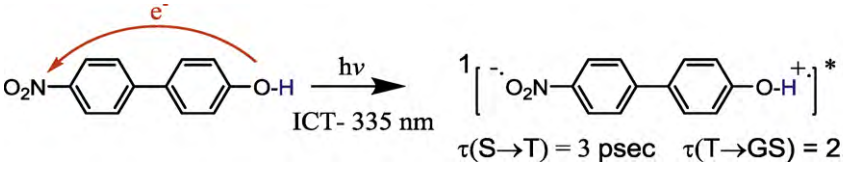

(19)

In organic solvents with a variety of added proton acceptor bases, H-bonded adducts form in equilibrium amounts as shown by IR and UV–vis spectral measurements, Eq. (20). For example, for *tert*-butylamine as base in DCE, λ_{max} shifts from 335 to 354 nm with $K_A = 104 \pm 10\ M^{-1}$ at $23 \pm 2\ ^\circ C$ from spectrophotometric measurements:

(20)

The adducts were of interest because of the spectral shifts with added base and the possibility of observing *photo*-EPT, Eq. (21):

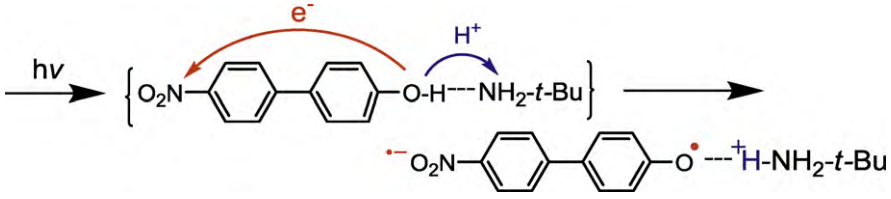

(21)

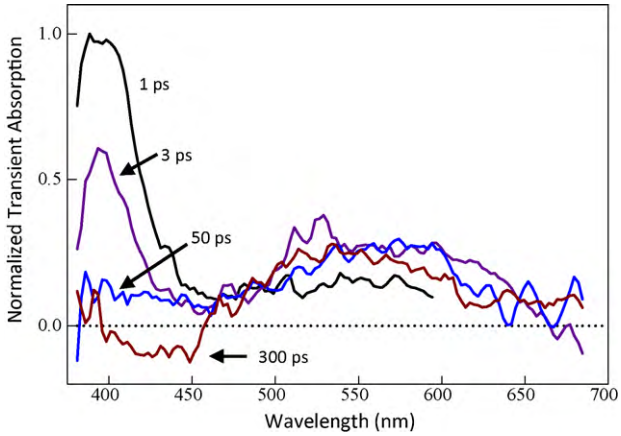

Fig. 6. Transient absorption difference spectra for the *p*-nitrophenyl-phenol-*tert*-butylamine adduct in 1,2-dichloroethane at 23 ± 3 °C, following 388 nm excitation at: 1, 3, 50, and 300 ps.

It is interesting to note that the proposed *photo*-EPT reaction in Eq. (21) is a photochemical analog of EPT oxidation of tyrosine Y_Z in Fig. 2, Eq. (22) [25,48,49]:

(22)

Spectral changes following ultrafast 388 nm (25,800 cm^{-1}) excitation of the *tert*-butylamine adduct are shown in Fig. 6 with observation times following excitation indicated on the figure.

Following 388 nm excitation, there is evidence for two intermediates. The first, observed at earliest times, ~250 fs, appears to be the deprotonated ground state $O_2N–O^-–{}^+HB$ (B = *tert*-butylamine) with λ_{max} = 410 nm shifted from λ_{max} = 466 nm for the anion, $O_2N–O^-$, due to H-bond stabilization. This assignment, which is supported by DFT calculations, shows that transfer of the proton occurs within 250 fs after excitation consistent with *photo*-EPT. Once formed, the photoproduct returns to the H-bonded adduct, $O_2N–O^-\cdots{}^+HB \rightarrow O_2N–O–H\cdots B$, with $\tau \sim 4.5$ ps.

A second intermediate is also observed, completely formed within 2 ps, which appears to be the corresponding triplet anion $^3(^{-\bullet}O_2N–O^{\bullet}\cdots{}^+HB)^*$ with λ_{max} = 550 nm. It undergoes proton loss within hundreds of picoseconds, $^3(^{-\bullet}O_2N–O^{\bullet}\cdots{}^+HB)^* \rightarrow {}^3(^{-\bullet}O_2N–O^{\bullet})^* + {}^+HB$, followed by decay of the triplet anion, $^3(^{-\bullet}O_2N–O^{\bullet})^* \rightarrow O_2N–O^-$, with τ = 15 ns.

These observations are consistent with the reaction scheme in Eqs. (23a–c), and the description of *photo*-EPT above. In this scheme, initial ICT excitation results in a ICT-EPT excited state with the transferring proton frozen in the equilibrium coordinate of the ν(O–H) ground state highly elongated in the ν(N–H) coordinate of the photoproduct. Equilibration along this proton transfer coordinate in the excited state occurs within 250 fs. There is a further complication in this case in that proton transfer is coupled to two competing electronic events: (1) rapid back electron transfer to give the deprotonated ground state. (2) singlet–triplet conversion to $^3(^{-\bullet}O_2N–O^{\bullet}\cdots{}^+HB)^*$.

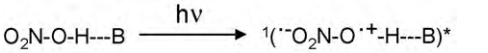

(23a)

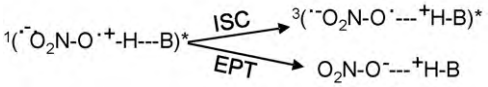

(23b)

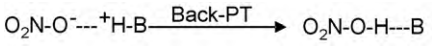

(23c)

Higher energy excitation of $O_2N–O–H\cdots B$ at 355 nm (28,200 cm^{-1}) with B = *tert*-butylamine results in an even more complex series of photo events. Both ground state photoproduct, $O_2N–O^-\cdots{}^+HB$, and singlet ICT excited state, $^1(^{-\bullet}O_2N–O^{\bullet}–H^+\cdots B)$ (λ_{max} = 440 nm) are observed. The singlet undergoes spin interconversion to the triplet ICT state ($\lambda_{max} \sim 600$ nm), $^1(^{-\bullet}O_2N–O^{\bullet}–H^+\cdots B) \rightarrow {}^3(^{-\bullet}O_2N–O^{\bullet}–H^+\cdots B)$, within 1–3 ps followed by proton transfer, $^3(^{-\bullet}O_2N–O^{\bullet}–H^+\cdots B) \rightarrow {}^3(^{-\bullet}O_2N–O^{\bullet}\cdots{}^+H–B)$, in 5–10 ps. The separated triplet anion, $^3(^{-\bullet}O_2N–O^{\bullet})$, appears hundreds of picoseconds later.

A possible explanation for the excitation wavelength dependence and rapid proton loss is suggested in the energy-coordinate diagram in Fig. 7. It describes ICT excited state energy-coordinate curves for $^1(n\pi^*\text{ICT})$, $^1(^{-\bullet}O_2N–O^{\bullet}–H^+\cdots B)$, and $^1(n\pi^*\text{ICT-EPT})$, $^1(^{-\bullet}O_2N–O^{\bullet}\cdots H^+–B)$ excited states with B = *tert*-butylamine. Low energy excitation at 388 nm is followed by the sequence in Eq. (23). Higher energy excitation at 355 nm gives both $^1(n\pi^*\text{ICT-EPT})$ and $^1(n\pi^*\text{ICT})$ excited states. The $^1(n\pi^*\text{ICT})$ state converts to $^1(n\pi^*\text{ICT-EPT})$ or undergoes spin interconversion to the H-bonded triplet followed by relatively slow proton transfer.

Evidence for photo-EPT has also been obtained in H-bonded base adducts between 1-methylimidazole and the coumarin laser dye 7-hydroxy-4-(trifluoromethyl) coumarin (F_3CCou–OH) by ultrafast measurements in toluene at room temperature [50]. The dye itself is weakly emissive. A 1:1 adduct with the base forms

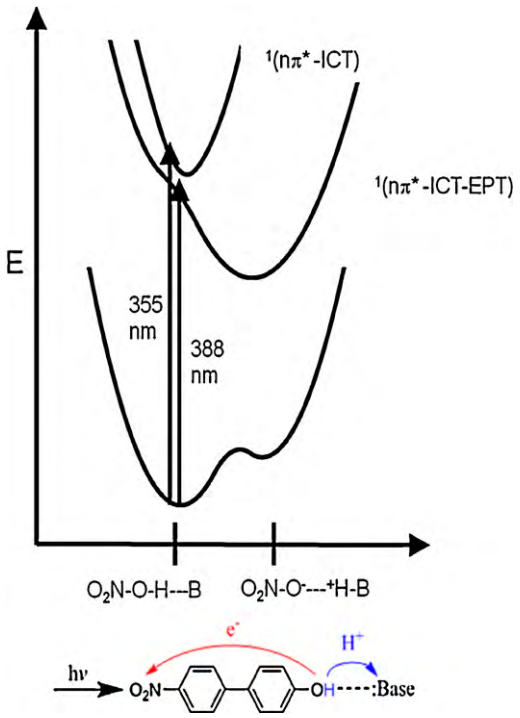

Fig. 7. Energy-coordinate curves illustrating 388 and 355 nm excitation of $O_2N–O–H\cdots B$ and the $^1(n\pi^*\text{ICT-EPT})$ and $^1(n\pi^*\text{EPT})$ excited states that result, see text.

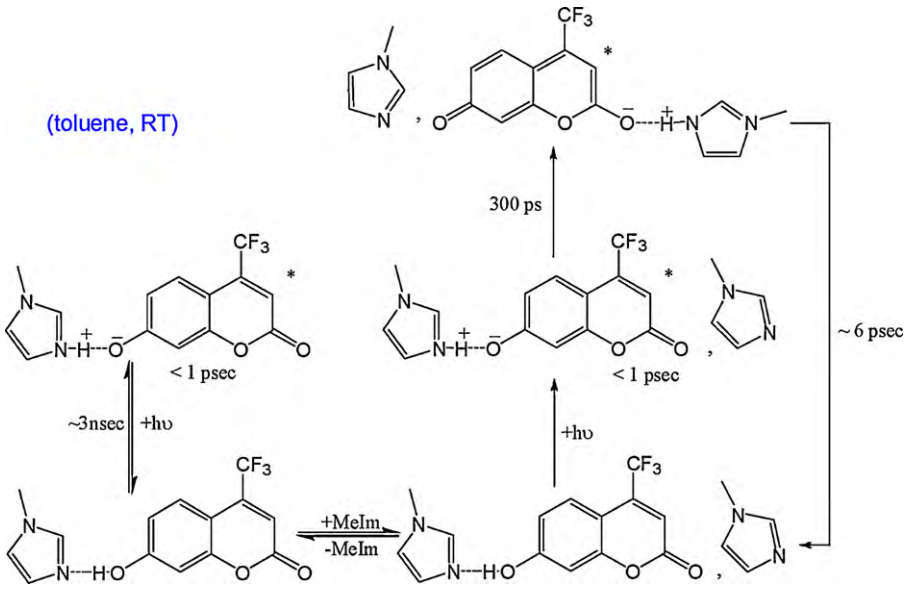

Fig. 8. Reaction scheme illustrating *photo*-EPT in the 1:1 adduct between 7-hydroxy-4-(trifluoromethyl) coumarin and 1-methylimidazole and conversion to the low energy tautomer in a 2:1 adduct in toluene at room temperature.

with $K_A \sim 2000\ M^{-1}$. Excitation of the adduct results in rapid, <1 ps, proton transfer with prompt emission observed from the highly fluorescent H-bonded anion at 460 nm, $\tau \sim 3$ ns. This a more straightforward example of photo-EPT since there is no complication from back electron transfer or spin change.

With higher concentrations of added base a new emission appears at 520 nm with $\tau \sim 6$ ns. It arises from the excited state tautomer shown in Fig. 8. At these higher concentrations higher adducts form inducing internal proton transfer within the adduct to give the lower energy tautomer excited state. The overall reaction scheme is illustrated in Fig. 8.

5.2. Electron proton transfer (EPT) quenching of metal-to-ligand charge transfer (MLCT) excited states

Metal-to-ligand charge transfer (MLCT) excited states have provided a paradigm for excited state electron transfer. The archetype is the MLCT excited state of $Ru(bpy)_3^{2+}$, $Ru(bpy)_3^{2+*}$. It provided the first experimental demonstration of excited state electron transfer and was shown to undergo both oxidative and reductive excited state electron transfer quenching with low kinetic barriers [4,10,46].

The redox potential diagram in Fig. 9 illustrates the effect of excitation on redox potentials. The excited state is a moderately strong oxidant, $E^{\circ'} = +0.8$ V, and reductant, $E^{\circ'} = -0.8$ V vs SCE in CH_3CN, $I = 0.1$. The diagram also illustrates that oxidative quenching to give $Ru(bpy)_3^{3+}$ produces a powerful oxidant capable of oxidizing water from pH 0 to 14 and reductive quenching a powerful reductant, $Ru(bpy)_3^{+}$, capable of water reduction.

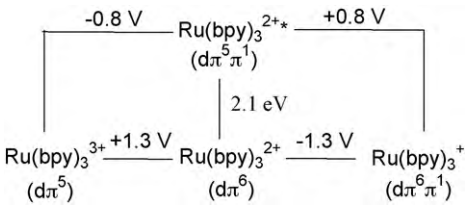

Fig. 9. Redox potential diagram for ground state and MLCT excited state redox potentials for $Ru(bpy)_3^{2+}$ in CH_3CN at room temperature, $I = 0.1$, vs SCE.

Even given the enhanced redox properties of the excited state, in solar fuel reactions mechanistic demands imposed by PCET and combined e^-/H^+ transfer must be met. To meet those demands we have begun a systematic investigation of MLCT excited states capable of undergoing EPT quenching. In these complexes, excited state electron transfer is combined with the ability to donate or accept protons as part of the quenching act. This has the effect of combining sequential excited state electron transfer followed by proton transfer into a single step to create thermodynamically powerful intermediates for EPT oxidation or reduction.

Excited state EPT reactivity was first demonstrated for reductive quenching of the lowest MLCT excited state of the mixed ligand complex $Ru(bpy)_2(bpz)^{2+}$ (bpz is 4,4′-bipyrazine) by hydroquinone, H_2Q. In the mixed ligand complex the lowest π^* acceptor level is on bpz and the lowest MLCT excited state is $Ru^{III}(bpy)_2(bpz^{\bullet -})^{2+*}$. In the ground state bpz has a low proton affinity with $pK_a = -1.6$. The pK_a increases to 4.4 in the excited state [51–53]:

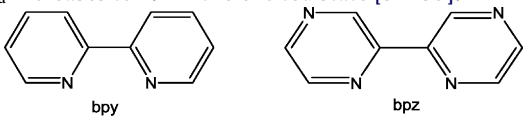

bpy and bpz

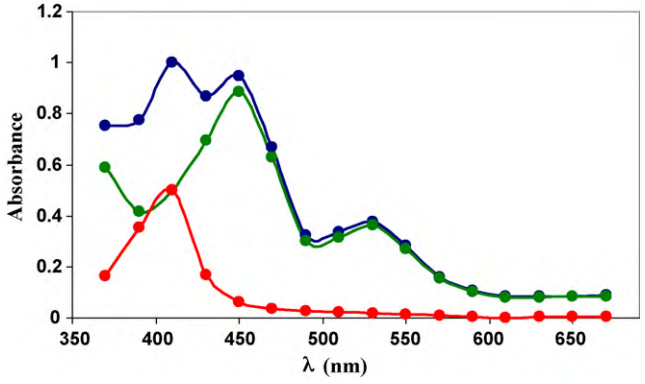

Fig. 10. Transient absorption difference spectrum (blue) obtained following 355 nm ns laser flash photolysis of $[Ru(bpy)_2(bpz)]^{2+}$ with 0.47 M H_2Q in 1:1 CH_3CN:H_2O, 0.1 M in KPF_6 at 23 ± 2 °C: blue, experimental spectrum; red, $HQ^{\bullet}$; green, $[(bpy)_2Ru(bpzH^{\bullet})]^{2+}$.

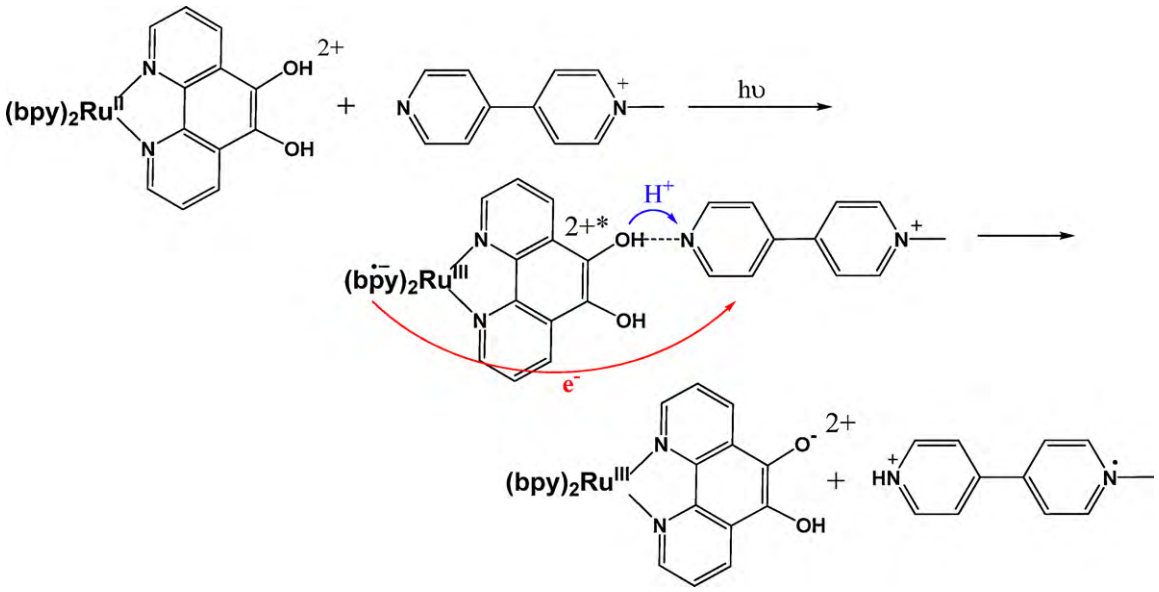

Fig. 11. Oxidative quenching of $[(bpy)_2Ru(phen(OH)_2]^{2+*}$ by p-$MeNC_6H_4$–$C_6H_4N^+$ in CH_3CN 0.1 M in tetra-n-butyl ammonium hexafluorophosphate at 23 ± °C.

As shown by the calculated $\Delta G^{\circ\prime}$ values in Eqs. (24a) and (24b), reductive quenching of $Ru^{III}(bpy)_2(bpz^{\bullet-})^{2+*}$ by H_2Q by EPT is favored over electron transfer by ~0.6 eV. This is a consequence of the enhanced acidity of $H_2Q^{+/\bullet}$ compared to H_2Q with $\Delta pK_a = 10.9$ [18] and of the increased basicity of the excited state compared to the ground state. Concerted EPT to $Ru^{III}(bpy)_2(bpz^{\bullet-})^{2+*}$ avoids high-energy intermediates formed by either initial ET or PT:

$$(bpy)_2Ru^{III}(bpz^{\cdot-})^{2+*} + H_2Q \xrightarrow{ET} (bpy)_2Ru^{II}(bpz^{\cdot-})^{+} + H_2Q^{\cdot+}$$
$$\Delta G^{\circ} = +0.06\,eV \quad (24a)$$

$$(bpy)_2Ru^{III}(bpz^{\cdot-})^{2+*} + H_2Q \xrightarrow{EPT} (bpy)_2Ru^{II}(bpz^{\cdot}H)^{2+} + HQ^{\cdot},$$
$$\Delta G^{\circ} = +0.55\,eV \quad (24b)$$

Nanosecond transient absorption and transient EPR measurements in argon-deaerated 1:1 CH_3CN:H_2O (0.1 M KPF_6) at 23 ± 2 °C revealed the quenching mechanism in Scheme 5 [54]. As shown in Fig. 10, the transient absorption spectrum obtained 900 ns after the laser pulse provides clear evidence for the intermediates $HQ^{\bullet}$ and $Ru(bpy)_2(bpzH^{\bullet-})^{2+}$.

Lifetime and emission quenching experiments over a range of H_2Q concentrations established the mechanism in Scheme 5. In this mechanism pre-association occurs between the excited state $Ru^{III}(bpy)_2(bpz^{\bullet-})^{2+*}$ and H_2Q with $K_A = 10 \pm 1\,M^{-1}$. Adduct formation is followed by excited state quenching with appearance of the EPT products $HQ^{\bullet}$ and $Ru(bpy)_2(bpzH^{\bullet-})^{2+}$

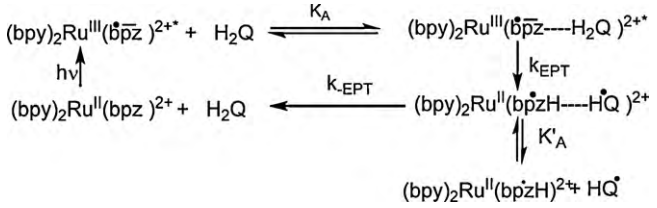

Scheme 5. Excited state EPT quenching of $Ru(bpy)_2(bpz)^{2+*}$ by hydroquinone.

immediately following the flash. For the quenching step, $[(bpy)_2Ru^{III}(bpz^{\bullet-})^{2+*}\cdots H_2Q] \rightarrow [(bpy)_2Ru^{II}(bpzH^{\bullet})^{2+}\cdots HQ^{\bullet}]$, $k_{EPT} = (4.5 \pm 0.1 \times 10^6\,s^{-1})$ with $k_{EPT}\,(H_2O)/k_{EPT}(D_2O) = 1.81 \pm 0.06$.

The reduced complex $[(bpy)_2Ru(bpzH^{\bullet})^{2+}$ is a powerful EPT reducing agent with $E^{\circ\prime} = -0.77$ V vs NHE for the $[Ru(bpy)_2(bpz)]^{2+}/[(bpy)_2Ru(bpzH^{\bullet})^{2+}$ couple [53]. In an initial study of its reactivity it was shown to undergo EPT with benzoquinone acting as the electron–proton acceptor, Eq. (25), with $k = 8.5 \pm 0.1 \times 10^8\,M^{-1}\,s^{-1}$. EPT reduction was followed by disproportion of $HQ^{\bullet}$ with $k = 2.9 \pm 0.1 \times 10^5\,M^{-1}\,s^{-1}$, Eq. (26). Similarly, the reduced complex was shown to react with added benzaldehyde with $k(H_2O) = 2.2 \pm 0.3 \times 10^6\,M^{-1}\,s^{-1}$.

$$[(bpy)2Ru^{II}(bpzH^{\bullet})]^{2+} + Q \rightarrow [(bpy)_2Ru^{II}(bpz)]^{2+} + HQ^{\bullet} \quad (25)$$

$$2HQ^{\bullet} \rightarrow H_2Q + Q \quad (26)$$

We have demonstrated a similar pathway for oxidative quenching. In one series of experiments oxidative quenching of the MLCT excited state of $[(bpy)_2Ru(phen(OH)_2]^{2+}$ ($phen(OH)_2$ is 1,10-phenanthroline-5,6-diol) by mono-methylated 4,4′-bipyridinium cation (p-$MeNC_6H_4$–$C_6H_4N^+$) has also been shown to occur by EPT, Fig. 11. In this reaction, EPT and concerted e^-/H^+ transfer occur from excited state to quencher to give the protonated $MV^{\bullet+}$ analog, p-$MeNC_6H_4$–$C_6H_4NH^{\bullet+}$. The appearance of the EPT products is easily discernible by the appearance of characteristic $MV^{\bullet+}$-like absorptions at ~400 and 600 nm for the latter. Oxidative EPT quenching in this case results in a powerful oxidant $[(bpy)_2Ru^{III}(phen(OH)(O^-)]^{2+}$ with implied reactivity as a H-atom or EPT oxidant.

The implied reactivity of the photoproduced transients from reductive and oxidative quenching is impressive but yet to be fully exploited. In experiments currently in progress we are exploring this aspect of this emerging area of photochemistry.

6. Conclusions

At the heart of photosynthesis and associated schemes for making solar fuels is a requirement for coupling light absorption and excited state/exciton formation with chemical reactions involving multi-electron/multi-proton change. In photosynthesis this occurs by a complex set of coupled electron/proton transfers driven by

light absorption and local free energy gradients created by excited state electron transfer. Photosystem II is imbedded in the thylakoid membrane. In its structure there are complex and intricate pathways for meeting the local proton demands of concerted electron–proton transfer (EPT) and long-range proton transfer.

Considerable simplification in design is available in dye sensitized photoelectrochemical synthesis cells (DS-PEC) by application of a modular approach. In this approach light absorption and excited state formation at a semiconductor interface are followed by electron injection, build up of oxidative equivalents, and proton release at a photoanode where water oxidation occurs. Reductive equivalents are delivered to a second electrode for water/H^+ or CO_2 reduction with proton transfer through a solution or membrane interface.

Even further simplification may be available by exploiting photochemical electron-proton tranfer (*photo*-EPT) in which light excitation results in electron transfer followed by proton transfer before relaxation occurs. Simultaneous transfer of both e^-/H^+ can lead directly to highly reactive intermediates for H-atom/EPT pathways.

Acknowledgments

Acknowledgments are made for support of this research as part of the UNC EFRC: Solar Fuels and Next Generation Photovoltaics, an Energy Frontier Research Center funded by the U.S. Department of Energy, Office of Science, Office of Basic Energy Sciences under Award Number DE-SC0001011. Funding was also provided by the National Science Foundation (Grants CHE0645890 and CHE0809045) and the Department of Energy (Grant DE-FG02-06ER15788) and is gratefully acknowledged.

References

[1] W. Rüttinger, G.C. Dismukes, Chem. Rev. 97 (1997) 1.
[2] J. Barber, B. Anderson, Nature 370 (1995) 31.
[3] A.C. Benniston, A. Harriman, Mater. Today 11 (2008) 26.
[4] J.H. Alstrum-Acevedo, M.K. Brennaman, T.J. Meyer, Inorg. Chem. 44 (2005) 6802.
[5] V. Balzani, A. Credi, M. Venturi, ChemSusChem 1 (2008) 26.
[6] R. Lomoth, A. Magnuson, M. Sjödin, P. Huang, S. Styring, L. Hammarström, Photosynth. Res. 87 (2006) 25.
[7] S. Fukuzumi, Eur. J. Inorg. Chem. 9 (2008) 1351.
[8] M.R. Wasielewski, J. Org. Chem. 71 (2006) 5051.
[9] M. Medina, FEBS J. 276 (2009) 3942.
[10] V. Balzani, Photochem. Photobiol. Sci. 2 (2003) 459.
[11] A.J. Bard, M.A. Fox, Acc. Chem. Res. 28 (1995) 141.
[12] V.K. Yachandra, K. Sauer, M.P. Klein, Chem. Rev. 96 (1996) 2927.
[13] G. Renger, T. Renger, Photosynth. Res. 98 (2008) 53.
[14] J. Kern, G. Renger, Photosynth. Res. 94 (2007) 183.
[15] F. Liu, J.J. Concepcion, J.W. Jurss, T. Cardolaccia, J.L. Templeton, T.J. Meyer, Inorg. Chem. 47 (2008) 1727.
[16] M.R. Wasielewski, Chem. Rev. 92 (1992) 435.
[17] T.J. Meyer, M.H.V. Huynh, Inorg. Chem. 43 (2003) 8140.
[18] R.A. Binstead, M.E. McGuire, A. Dovletoglou, W.K. Seok, L.E. Roecker, T.J. Meyer, J. Am. Chem. Soc. 114 (1992) 173.
[19] B.A. Moyer, T.J. Meyer, J. Am. Chem. Soc. 100 (1978) 3601.
[20] M.H.V. Huynh, T.J. Meyer, Chem. Rev. 107 (2007) 5004.
[21] K.J. Takeuchi, G.J. Samuels, S.W. Gersten, J.A. Gilbert, T.J. Meyer, Inorg. Chem. 22 (1983) 1407.
[22] C.J. Fecenko, H.H. Thorp, T.J. Meyer, J. Am. Chem. Soc. 129 (2007) 15098.
[23] C.J. Fecenko, T.J. Meyer, H.H. Thorp, J. Am. Chem. Soc. 128 (2006) 11020.
[24] C.F. Murphy, C.J. Gagliardi, H.H. Thorp, T.J. Meyer, in preparation.
[25] T.J. Meyer, M.H.V. Huynh, H.H. Thorp, Angew. Chem. Int. Ed. 46 (2007) 5284.
[26] L. Taiz, E. Zeiger, Plant Physiology, 4th ed., Sinauer Associates Inc., 2006.
[27] B. Loll, B. Kern, W. Saenger, A. Zouni, J. Biesiadka, Nature 438 (2005) 1040.
[28] J. Yano, J. Kern, K. Sauer, M.J. Latimer, Y. Pushkar, J. Biesiadka, B. Loll, W. Saenger, J. Messinger, A. Zouni, V.K. Yachandra, Science 314 (2006) 821.
[29] Thykaloid membrane, Wikipedia, http://upload.wikimedia.org/wikipedia/commons/1/18/Thylakoid_membrane.png (10.28.09).
[30] K.N. Ferreira, T.M. Iverson, K. Maghaoui, J. Barber, S. Iwata, Science 303 (2004) 1831.
[31] R.A. Roffey, D.M. Kramer, Govindjee, R.T. Sayre, Biochim. Biophys. Acta 1185 (1994) 257.
[32] F. Mamedov, R.T. Sayre, S. Styring, Biochemistry 37 (1998) 14245.
[33] B. Svensson, C. Etchebest, P. Tuffery, P. van Kan, J. Smith, S. Styring, Biochemistry 35 (1996) 14486.
[34] C.F. Baes Jr., R.E. Messmer, The Hydrolysis of Metal Cations, R.E. Kreiger, Malabar, FL, 1986.
[35] D.D. Perrin, Dissociation Constants of Inorganic Acids and Bases in Aqueous Solution, Butterworths, London, 1969.
[36] G.T. Higgins, B.V. Bergeron, G.M. Hasselmann, F. Farzad, G.J. Meyer, J. Phys. Chem. B 110 (2006) 2598.
[37] B. O'Regan, M. Grätzel, Nature 353 (1991) 737.
[38] Md.K. Nazeeruddin, C. Klein, P. Liska, M. Grätzel, Coord. Chem. Rev. 249 (2005) 1460.
[39] Z. Chen, J.J. Concepcion, J.W. Jurss, T.J. Meyer, J. Am. Chem. Soc. 131 (2009) 15580.
[40] J.J. Concepcion, J.W. Jurss, P.G. Hoertz, T.J. Meyer, Angew. Chem. Int. Ed. 48 (2009) 9473.
[41] J.A. Treadway, J.A. Moss, T.J. Meyer, Inorg. Chem. 38 (1999) 4386.
[42] W.J. Youngblood, S.-H.A. Lee, Y. Kobayashi, E.A. Hernandez-Pagan, P.G. Hoertz, T.A. Moore, A.L. Moore, D. Gust, T.E. Mallouk, J. Am. Chem. Soc. 131 (2009) 926.
[43] J.J. Concepcion, J.W. Jurss, M.K. Brennaman, P.G. Hoertz, A.O.T. Patrocinio, N.Y.M. Iha, J.L. Templeton, T.J. Meyer, Acc. Chem. Res. 42 (2009) 1954.
[44] S. Hammes-Schiffer, A.V. Soudackov, J. Phys. Chem. B 112 (2008) 14108.
[45] S.J. Edwards, A.V. Soudackov, S. Hammes-Schiffer, J. Phys. Chem. A 113 (2009) 2117.
[46] L.M. Tolbert, K.M. Solntsev, Acc. Chem. Res. 35 (2002) 19.
[47] B.C. Westlake, J.J. Paul, M.K. Brennaman, J.J. Concepcion, T.J. Meyer, J.M. Papanikolas, in preparation.
[48] C.W. Hoganson, G.T. Babcock, Science 277 (1997) 1953.
[49] C. Tommos, G.T. Babcock, Acc. Chem. Res. 31 (1998) 18.
[50] B.C. Westlake, J.J. Paul, S.E. Bettis, S.D. Hampton, T.J. Meyer, J.M. Papanikolas, in preparation.
[51] A. Rugge, C.D. Clark, M.Z. Hoffman, D.P. Rillema, Inorg. Chim. Acta 2791 (1998) 200.
[52] H. Sun, M.Z. Hoffman, J. Phys. Chem. 97 (1993) 5014.
[53] M. D'Angelantonio, Q.G. Mulazzani, M. Venturi, M. Ciano, M.Z. Hoffman, J. Phys. Chem. 95 (1991) 5121.
[54] J.J. Concepcion, M.K. Brennaman, J.R. Deyton, N.V. Lebedeva, M.D.E. Forbes, J.M. Papanikolas, T.J. Meyer, J. Am. Chem. Soc. 129 (2007) 6968.